



**HAL**  
open science

# The differential solvent exposure of N-terminal residues provides ‘fingerprints’ of alpha-synuclein fibrillar polymorphs

Maud Landureau, Virginie Redeker, Tracy Bellande, Stéphanie Eyquem,  
Ronald Melki

## ► To cite this version:

Maud Landureau, Virginie Redeker, Tracy Bellande, Stéphanie Eyquem, Ronald Melki. The differential solvent exposure of N-terminal residues provides ‘fingerprints’ of alpha-synuclein fibrillar polymorphs. *Journal of Biological Chemistry*, 2021, 296, pp.100737. 10.1016/j.jbc.2021.100737 . cea-03219237

**HAL Id: cea-03219237**

**<https://cea.hal.science/cea-03219237>**

Submitted on 25 Nov 2021

**HAL** is a multi-disciplinary open access archive for the deposit and dissemination of scientific research documents, whether they are published or not. The documents may come from teaching and research institutions in France or abroad, or from public or private research centers.

L’archive ouverte pluridisciplinaire **HAL**, est destinée au dépôt et à la diffusion de documents scientifiques de niveau recherche, publiés ou non, émanant des établissements d’enseignement et de recherche français ou étrangers, des laboratoires publics ou privés.



Distributed under a Creative Commons Attribution 4.0 International License



# The differential solvent exposure of N-terminal residues provides “fingerprints” of alpha-synuclein fibrillar polymorphs

Received for publication, February 4, 2021, and in revised form, April 15, 2021. Published, Papers in Press, April 30, 2021.

<https://doi.org/10.1016/j.jbc.2021.100737>

Maud Landureau<sup>1</sup>, Virginie Redeker<sup>1,\*</sup> , Tracy Bellande<sup>1</sup>, Stéphanie Eyquem<sup>2</sup>, and Ronald Melki<sup>1</sup>

From the <sup>1</sup>Laboratory of Neurodegenerative Diseases, Institut Francois Jacob (MIRCen), CNRS, CEA, University Paris-Saclay, Fontenay-Aux-Roses Cedex, France; <sup>2</sup>Sanofi R&D, Rare & Neurologic Diseases Research Therapeutic Area, Neurodegeneration Research, Chilly Mazarin, France

Edited by Paul Fraser

Synucleinopathies are neurodegenerative diseases characterized by the presence of intracellular deposits containing the protein alpha-synuclein (aSYN) within patients' brains. It has been shown that aSYN can form structurally distinct fibrillar assemblies, also termed polymorphs. We previously showed that distinct aSYN polymorphs assembled *in vitro*, named fibrils, ribbons, and fibrils 91, differentially bind to and seed the aggregation of endogenous aSYN in neuronal cells, which suggests that distinct synucleinopathies may arise from aSYN polymorphs. In order to better understand the differential interactions of aSYN polymorphs with their partner proteins, we mapped aSYN polymorphs surfaces. We used limited proteolysis, hydrogen–deuterium exchange, and differential antibody accessibility to identify amino acids on their surfaces. We showed that the aSYN C-terminal region spanning residues 94 to 140 exhibited similarly high solvent accessibility in these three polymorphs. However, the N-terminal amino acid residues 1 to 38 of fibrils were exposed to the solvent, while only residues 1 to 18 within fibrils 91 were exposed, and no N-terminal residues within ribbons were solvent-exposed. It is likely that these differences in surface accessibility contribute to the differential binding of distinct aSYN polymorphs to partner proteins. We thus posit that the polypeptides exposed on the surface of distinct aSYN fibrillar polymorphs are comparable to fingerprints. Our findings have diagnostic and therapeutic potential, particularly in the prion-like propagation of fibrillar aSYN, as they can facilitate the design of ligands that specifically bind and distinguish between fibrillar polymorphs.

Parkinson's disease (PD), multiple system atrophy (MSA), and dementia with Lewy bodies (DLB) are characterized by the presence of aSYN-rich deposits within the central and peripheral nervous systems (1, 2).

The protein aSYN is abundant in the brain, especially in neurons, where it is involved in the regulation of synaptic vesicle release and trafficking (3–5). aSYN N-terminal 60 amino acid residues form a domain that can adopt an alpha-

helical structure upon binding to lipid vesicles (6, 7). The amino acid residues stretch 61 to 95 is hydrophobic and prone to form amyloid fibrils. It is named the nonamyloid- $\beta$  component domain (8). The C-terminal extremity, from the amino acid residues 96 to 140, is negatively charged. It binds metal ions and protein partners (9). Monomeric alpha-synuclein is flexible and can adopt multiple conformations depending on its environment or partners (10).

In synucleinopathies, beta-strands-rich aSYN conformations stack into fibrillar assemblies (11). These assemblies are able to elongate by recruitment of monomeric aSYN. This phenomenon is named seeding (8, 12–14). These aggregates can trap other proteins or lipids and affect their physiological activities (15). Furthermore, alpha-synuclein aggregates alter cellular homeostasis and proteostasis and compromise the integrity of organelles leading to neurodegeneration and chronic inflammation (16–18). Numerous studies have shown that fibrils traffic between cells. The fibrils seed the aggregation of endogenous aSYN within naïve cells. This is believed to be at the origin of prion-like propagation within the brain (12).

Distinct synucleinopathies affect different brain regions and cell types. They progress at different rates and exhibit distinct symptoms (19, 20). The existence of aSYN assemblies with distinct structures, named strains by analogy with different prion diseases (21), has been proposed to account for different synucleinopathies, and evidences supporting this working hypothesis have been brought (22, 23). Furthermore, an increasing number of reports suggest that aSYN aggregates in the brain of patients with MSA, DLB or PD are structurally distinct (24–26).

We previously established stringent experimental conditions under which aSYN assembles into pure structurally distinct fibrillar polymorphs we named fibrils, ribbons, and fibrils 91 (22, 27, 28). These fibrillar polymorphs have characteristic shapes in transmission electron microscopy (TEM), different physical properties as documented by atomic force microscopy (28), different secondary structure contents and distributions as assessed by solid-state nuclear magnetic resonance spectroscopy (ssNMR), and different proteolytic profiles (22, 27, 29, 30). We further established a structure–function relationship by

\* For correspondence: Virginie Redeker, [virginie.redeker@cnrs.fr](mailto:virginie.redeker@cnrs.fr).

## Surface mapping of alpha-synuclein strains

showing that the structural differences between polymorphs impact their ability to bind neuronal cells (31), seed the aggregation of endogenous aSYN, spread within the central nervous system, and impact the motor behavior of affected animals (23, 32).

Recent developments in cryo-electron microscopy (cryo-EM) allow determining to an atomic resolution the structure of the rigid core of fibrillar assemblies (33). This method allows neither identifying all the amino acid stretches exposed to the solvent at the surfaces of fibrillar assemblies nor determining how are regions less rigid than the amyloid core organized around it within those assemblies.

The polypeptide stretches exposed at the surfaces of fibrillar polymorphs define their protein and lipid interactomes. It is therefore of utmost importance to define them at the highest possible resolution to better understand what underlies their

differential binding to neuronal cells, resistance to clearance, and spread (31, 32).

Here we identify the amino acid stretches exposed to the solvent at the surface of aSYN fibrillar polymorphs fibrils, ribbons, and fibrils 91. We used limited proteolysis (34, 35) followed by western blotting with specific anti-aSYN antibodies and mass spectrometry (MS) to determine regions from different fibrillar polymorphs exposed to the solvent. We next strengthened our results by determining solvent accessibility at the amino acid level by performing hydrogen–deuterium exchange coupled with MS measurements (36, 37).

We demonstrate that aSYN C-terminal amino acid stretch 94 to 140 is highly accessible to the solvent in all three fibrillar polymorphs. This contrasts with the polymorphs-dependent differential exposure of aSYN N-terminal domain. Indeed, while aSYN amino acid stretch 1 to 38 is exposed to the

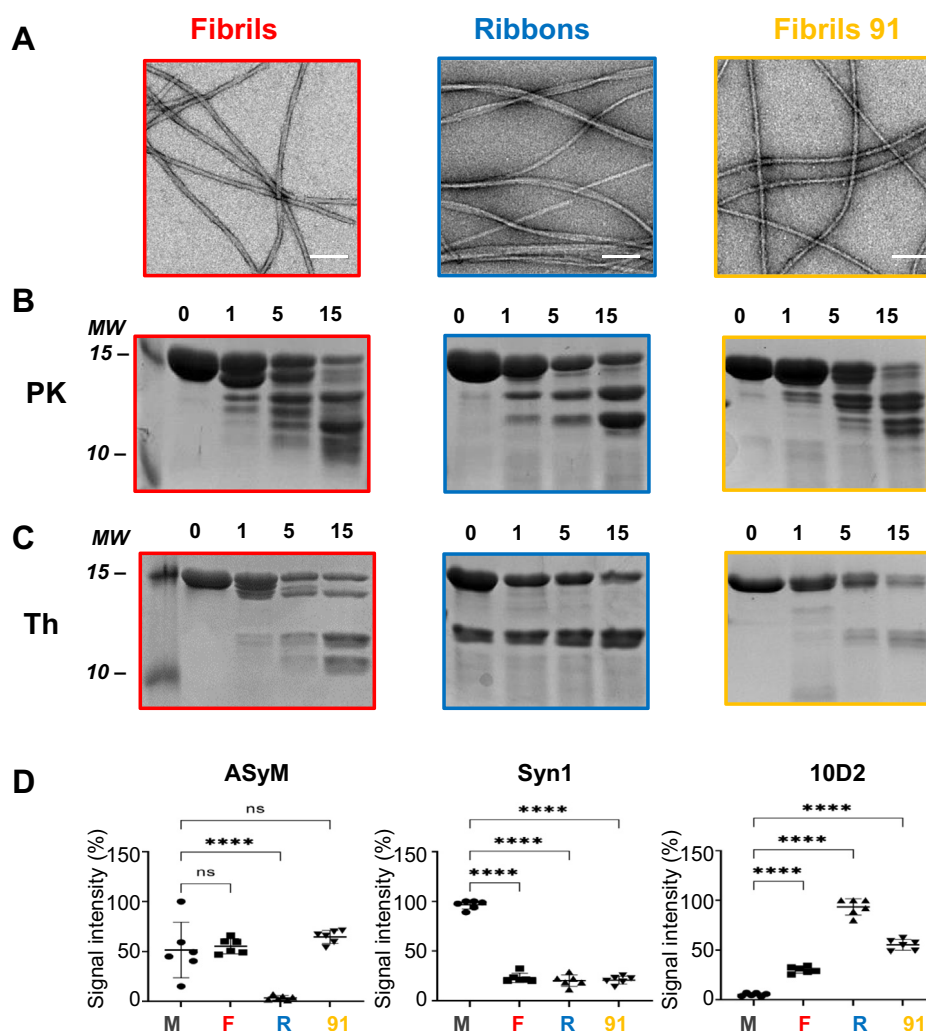


**Figure 1. Characterization of alpha-synuclein fibrillar polymorphs.** A, transmission electron micrographs of aSYN fibrillar polymorphs fibrils (red frame), ribbons (blue frame), and fibrils 91 (yellow frame), scale bar: 100 nm. B, proteinase K (PK, 3.8 µg/ml) and (C) thermolysin (Th, 5 µg/ml) degradation patterns of aSYN fibrillar polymorphs fibrils, ribbons, and fibrils 91 (100 µM monomer concentration) monitored over time on Coomassie stained SDS-PAGE (15%). Time (min) and molecular weight markers (MW, kDa) are shown on the top and left sides of the gels, respectively. D, comparative assessment of the binding of the antibodies ASyM, Syn1, and 10D2, directed against amino acid stretches 1 to 15, 91 to 99, and 118 to 127, respectively, to aSYN monomers, fibrils, ribbons, and fibrils 91 by dot-blot analysis performed in triplicate. The error bars represent standard deviation. Statistical significance was verified one-way ANOVA followed by Dunnett's multiple comparisons test. Significant (\*\*\*\*corresponding to a  $p$ -value < 0.0001) and nonsignificant (ns corresponding to  $p$ -value > 0.05) differences are indicated.

solvent in the polymorph fibrils, it is fully inaccessible in ribbons and accessible in part (residues 1–18) in the polymorph fibrils 91. The differences we observe reflect differences in polypeptide folding.

Our findings pave the way to design ligands with diagnostic and therapeutic potential that target distinct aSYN accessible surfaces and are capable of distinguishing different aSYN strains.

## Results

### *aSYN fibrillar polymorphs characterization*

We used different experimental conditions to assemble human recombinant wild-type aSYN into the three distinct fibrillar polymorphs, fibrils, ribbons, and fibrils 91. The polymorph fibrils were obtained under physiological salt concentration (22), ribbons were formed in a buffer with a low salinity, and fibrils 91 were generated in a buffer with a high pH, as previously described (22, 27, 28).

The homogeneity and nature of the fibrillar polymorphs were first assessed by TEM (Fig. 1A). Fibrils and fibrils 91 had a cylindrical aspect with twists while ribbons appeared flat (22, 28).

We next subjected the three fibrillar polymorphs to limited proteolysis using proteinase K and thermolysin to assess their characteristic proteolytic profiles. Theoretically, proteinase K and thermolysin can cleave 78 and 54 peptide bonds within aSYN, respectively. These two unspecific proteases will cleave a subset of those peptide bonds under the experimental conditions we designed, within amino acid stretches exposed to the solvent at the surface of the different polymorphs.

Highly reproducible, strain-specific and protease-specific proteolytic profiles, comparable to fingerprints, were obtained after SDS-PAGE and staining with Coomassie blue (Fig. 1, B and C) under conditions where monomeric aSYN is degraded within 5 to 15 min into polypeptides with molecular weight lower than 12 kDa (Fig. S1). These results demonstrate unequivocally that structurally distinct fibrillar aSYN polymorphs expose to the solvent different polypeptide chains.

All resulting proteolytic reaction products appeared fibrillar upon assessment by TEM (Fig. S2). Their bundling propensity increased. All the proteolytic polypeptides were found in the pellet when proteinase K and thermolysin-treated fibrils, ribbons, and fibrils 91 were subjected to ultracentrifugation (Fig. S2). This demonstrates that aSYN polypeptides remain bound together within the fibrillar structures under our experimental conditions until denaturation. This further indicates that our proteolytic treatment only affects fibrils surfaces, not their amyloid core.

### *Differential accessibility of aSYN regions within fibrillar polymorphs to monoclonal antibodies*

We determined the accessibility of polypeptide stretches spanning aSYN primary structure to different antibodies in aSYN monomers, fibrils, ribbons, and fibrils 91. The different species were immobilized on nitrocellulose membranes that were exposed to monoclonal antibodies directed against aSYN

amino acid stretch 1 to 15 (ASyM), 91 to 99 (Syn1), and 118 to 127 (10D2) (Fig. 1D). ASyM bound all species except ribbons, which indicates that its epitope is involved in ribbon amyloid core, in agreement with solid-state NMR data we previously obtained (22, 27, 29, 30). The antibody 10D2 bound all fibrillar polymorphs, indicating that aSYN C-terminal end is exposed to the solvent, again in agreement with previous solid-state NMR data (22, 27, 29, 30). Interestingly, 10D2 binds fibrillar aSYN polymorphs better than its monomeric form, which either reflects a low affinity for aSYN C-terminal domain or a preferential binding to a conformation aSYN C-terminal domain adopts in fibrillar polymorphs. Syn1 was found to bind best monomeric aSYN. This agrees with the partial or full involvement of aSYN amino acid stretch 91 to 99 within the amyloid core of the fibrillar polymorphs we analyzed (22, 27, 29, 30).

### *Mapping of aSYN fibrillar polymorphs surfaces by limited proteolysis*

We next identified the polypeptides generated by limited proteolytic cleavage of aSYN fibrillar polymorphs by proteinase K and thermolysin using two approaches.

We first performed western blotting after limited proteolysis using the monoclonal antibodies ASyM, 5G4, 10C3, Syn1 (38), and 10D2 directed against aSYN amino acid stretches 1 to 15, 46 to 53, 98 to 105, 91 to 99, and 118 to 127, respectively (Fig. 2). Syn1 recognized all the bands seen after SDS-PAGE and staining with Coomassie blue. This indicates that the amino acid stretch 91 to 99 is present in all proteinase K and thermolysin cleavage products (Figs. 1 and 2). The presence or absence of ASyM, 5G4, 10C3, and 10D2 epitopes within the different proteolytic polypeptides was next assessed after membranes stripping and probing with the different antibodies.

The antibody ASyM bound all polypeptides derived from proteinase K treatment of the polymorph ribbons but not the polymorphs fibrils and fibrils 91 as confirmed by the merge of Syn1 and ASyM immunodetection (Fig. 2, A–C). We conclude from this observation that the amino acid stretch 1 to 15 is inaccessible to proteinase K in the polymorph ribbons while it is in the polymorphs fibrils and fibrils 91. The antibodies 5G4 and 10C3 bound all polypeptides identified by SDS-PAGE and by Syn1 after proteinase K treatment (Fig. 2, A–C). We conclude from this observation that the amino acid stretch 46 to 105 is inaccessible to proteinase K in all aSYN fibrillar polymorphs. Most proteolytic polypeptides lacked 10D2 antibody binding (Fig. 2, A–C), which indicates the amino acid stretch 118 to 127 is accessible to the protease and the polypeptides are C-terminally truncated.

The binding of ASyM, 5G4, 10C3, and 10D2 to aSYN fibrillar polymorphs fibrils, fibrils 91, and ribbons thermolysin cleavage products (Fig. 2, D–F) is in full agreement with the results obtained with proteinase K. It shows that the amino acid stretch 1 to 15 is inaccessible to thermolysin in aSYN polymorph ribbons while it is in the polymorphs fibrils and fibrils 91 that the amino acid stretch 46 to 105 is inaccessible

## Surface mapping of alpha-synuclein strains

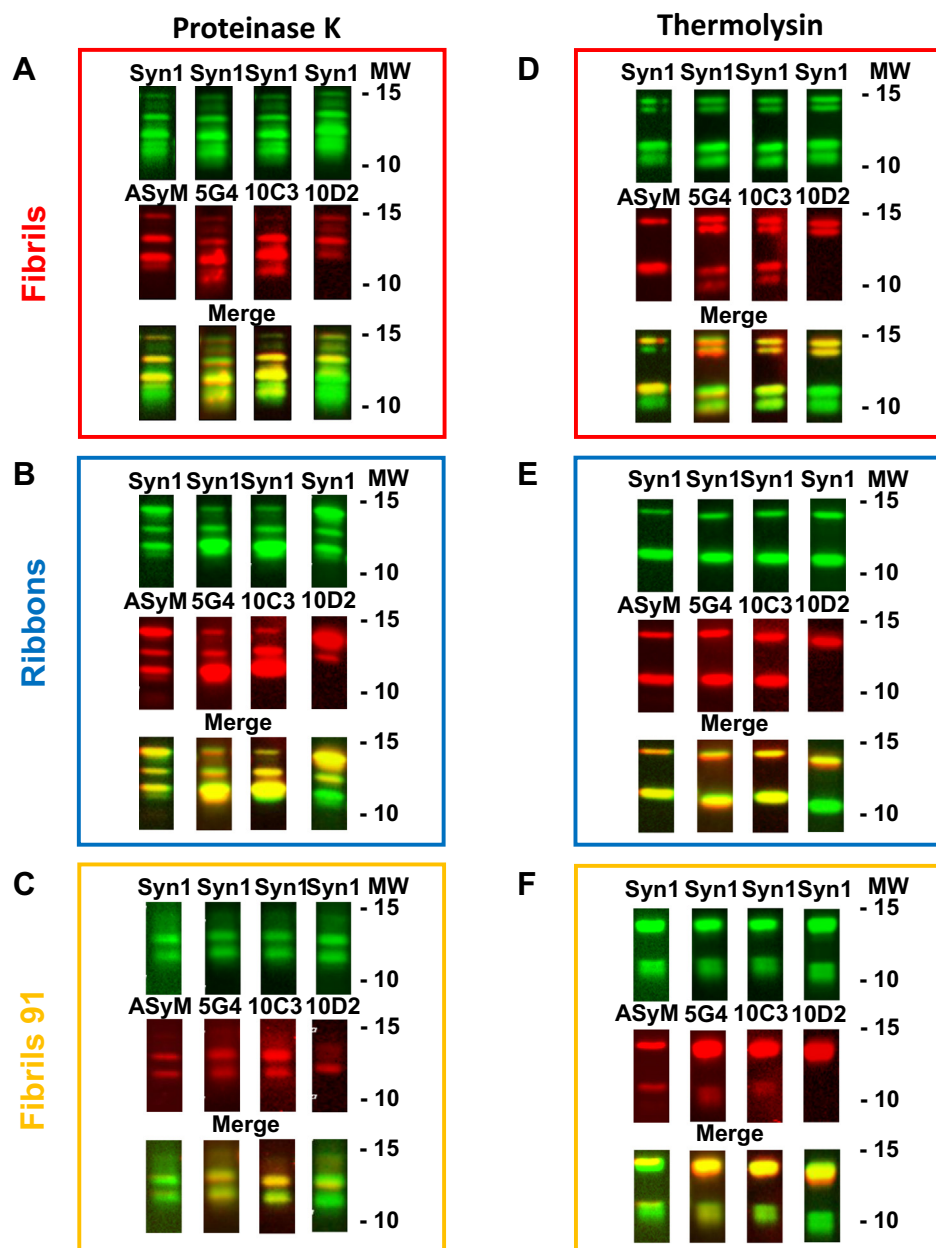


**Figure 2. Immunodetection of the proteolytic fragments generated after treatment of aSYN fibrillar polymorphs by proteinase K or thermolysin.** Fibrils (panels A and D, red frame), ribbons (panels B and E, blue frame), and fibrils 91 (panels C and F, yellow frame) were degraded by proteinase K (A–C) or thermolysin (D–F) for 15 min. The proteolytic fragments were identified by western blot analysis using the anti-aSYN antibodies Syn1, ASyM, 5G4, 10C3, and 10D2, epitopes of which span the amino acid stretches 91 to 99, 1 to 15, 46 to 53, 98 to 105, and 118 to 127. The molecular weight markers (MW, kDa) are shown on the left of each panel.

to thermolysin in all aSYN fibrillar polymorphs and that the amino acid stretch 118 to 127 is accessible to the protease in all aSYN fibrillar polymorphs.

Second, we identified all aSYN fibrillar polymorphs proteinase K and thermolysin cleavage products by MS. We used matrix-assisted laser desorption mass spectrometry (MALDI-MS) in the linear mode, with a sinapinic acid matrix given the apparent molecular weight of the polypeptides (>8000 Da). The MS spectra of the polypeptides generated after 15 min cleavage by proteinase K and thermolysin are displayed in Figure 3. Their identity, established in accordance to aSYN N- and C-terminal domains accessibility we observed by

immunodetection, and their mass accuracy are listed in Tables S1 and S2, respectively. The specific MALDI-MS proteolytic profile we observe for each aSYN strain is represented as a bar code, schematizing their exposure to the proteolytic enzymes (Fig. 3).

These data clearly demonstrate that the C-terminal polypeptide stretch 112 to 140 is highly accessible to proteolysis in all fibrillar aSYN strains (Fig. 3). Our data also show that the aSYN N-terminal polypeptide stretch 1 to 18 (Fig. 3) is inaccessible in the polymorphs ribbons while it is in fibrils and fibrils 91, and the polypeptide 1 to 30 is accessible only in the polymorph fibrils. Small polypeptides (<4000 Da) resulting

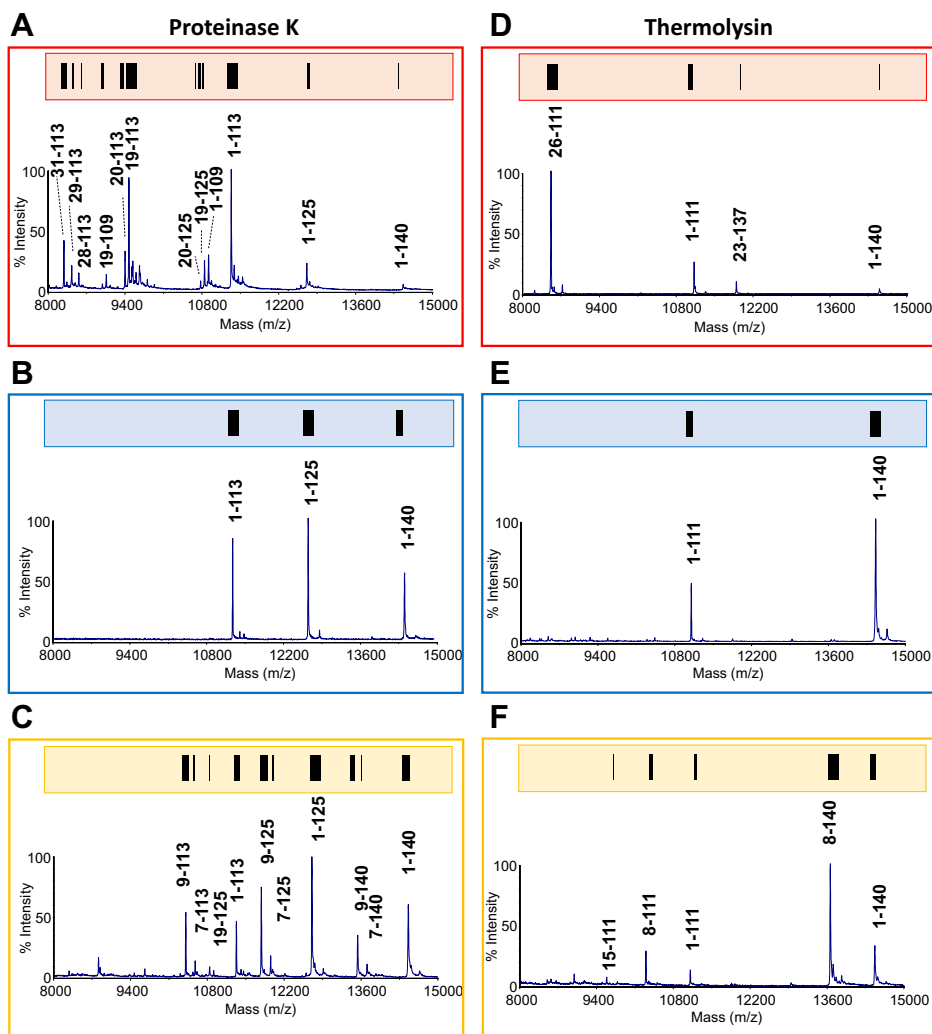


**Figure 3. Identification of the proteolytic fragments generated by treatment of aSYN fibrillar polymorphs by proteinase K and thermolysin by mass spectrometry.** Fibrils (red), ribbons (blue), and fibrils 91 (yellow) were degraded by proteinase K (A–C) or thermolysin (D–F) for 15 min. MALDI-MS mass spectra of long polypeptides are presented. The identity of each ion is given. Monoprotinated average masses of annotated peptide ions are given in Tables S1 and S2 for proteinase K and thermolysin digestions products, respectively. The specific MALDI-MS proteolytic profile of each aSYN strain is represented as a bar code on the top of the corresponding mass spectrum where the intensity of each ion is taken into account.

from limited proteolysis of fibrillar aSYN polymorphs by proteinase K and thermolysin were identified by MALDI-MS using HCCA as matrix and in reflectron mode. Proteinase K and thermolysin treatment yielded abundant short C-terminal peptides complementary to the large polypeptides: the 126 to 140 peptide (at  $MH^+$  1773.75 Da and  $MNa^+$  at 1795.73 Da) and 112 to 140 peptide (at  $MH^+$  = 3375.36 Da,  $MNa^+$  = 3397.49 Da) after proteinase K and thermolysin treatment, respectively. No abundant N-terminal polypeptides were detected, most probably because additional cleavages occurred and produced N-terminal peptides too small to be detected in the analyzed mass range.

The differential exposure to the solvent of aSYN polypeptide chain within the fibrillar polymorphs fibrils, ribbons, and fibrils 91 derived from the proteolytic cleavage assessment we performed is summarized in Figure 4. Altogether, our data indicate that aSYN C-terminal end is exposed in a similar manner to the solvent and therefore accessible to proteases in the three

structurally distinct fibrillar polymorphs. This contrasts with the N-terminal end that appears exposed to different extent in the polymorphs fibrils and fibrils 91 but not in ribbons.

#### Mapping of aSYN fibrillar surfaces by hydrogen–deuterium exchange

To further strengthen our results, we performed hydrogen–deuterium exchange experiments coupled to MALDI-MS measurements (HDX-MS). Indeed, the backbone amide hydrogen atoms of proteins exchange continuously with the hydrogen atoms from the solvent. HDX allows assessing how “labile” protein regions are. HDX correlates with the formation of secondary structure elements. Slow exchange is typically a consequence of H-bond formation in structured regions such as an amyloid core (36).

We first optimized the HDX-MS strategy so that rapid and efficient digestion of different aSYN fibrillar polymorphs and aSYN monomers yields peptides with similar masses. We

## Surface mapping of alpha-synuclein strains

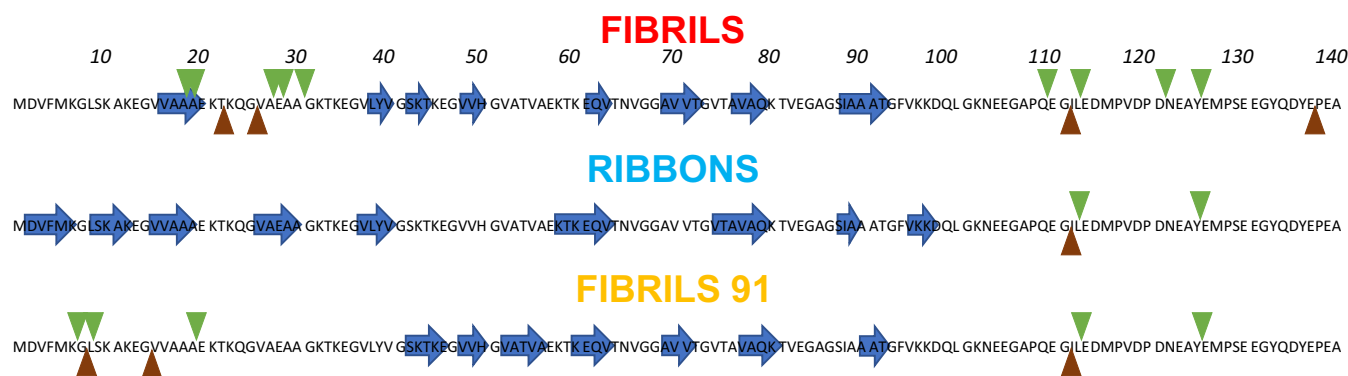


**Figure 4. Graphic representation of proteolytic accessibility of aSYN within the fibrillar polymorphs fibrils, ribbons, and fibrils 91.** The accessible cleavage sites of proteinase K (green arrows) and thermolysin (brown arrows) are indicated along aSYN primary structure for each fibrillar polymorph. Blue arrows represent amino acid stretches that adopt beta strand conformation we previously determined by NMR (27, 29, 30).

obtained, based on exact mass measurements by MALDI-MS of peptides generated following treatment of the different fibrillar polymorphs by pepsin (enzyme-to-protein ratio of 100:1) after HDX, a sequence coverage of 98% and 97% for aSYN monomers and fibrillar polymorphs, respectively (Table S3). The identity of the pepsin-derived peptides, both protonated and with sodium adducts, was confirmed by CID fragmentation of nondeuterated samples using both nanoLC-MSMS and MALDI-MSMS (Fig. S3). The peptide ions used for HDX measurements were those with a sodium adduct as they are much better detected and more abundant as mono-protonated peptides. We confirmed that the HDX with or without sodium adduct was similar for several abundant peptides.

HDX kinetics were derived from aSYN monomers and fibrillar polymorphs incubation for 2, 30, and 120 min in a deuterium (D<sub>2</sub>O) buffer. Monomeric aSYN pepsin-derived peptides exhibited 70 to 100% deuterium incorporation after 2 min incubation in D<sub>2</sub>O. HDX measurements were performed on partially assembled aSYN fibrillar polymorphs so that pepsin-derived peptides originating from aSYN monomers can be used as internal controls within any given HDX mass spectrum (Fig. S4). All peptides involved in H-bond formation and protected from the solvent within an aSYN fibrillar polymorph will yield bimodal spectral distributions of isotopic envelopes under our experimental conditions. The first isotopic envelope represents the peptide protected within the fibrillar polymorph while the second isotopic envelope originates from the corresponding peptide from monomeric aSYN, as previously observed (37). In contrast, peptides that are labile or exposed at the surfaces of aSYN fibrillar polymorphs exhibit unimodal spectral distributions of isotopic envelopes given they exchange equally well in aSYN monomers and fibrillar polymorphs. The maximal deuterium incorporation was reached within 30 min for most of the pepsin-derived peptides we analyzed (Fig. S5). The different pepsin-derived peptides from aSYN fibrillar polymorphs exhibited deuterium incorporation levels ranging from 1 to 100% after 30 min incubation in D<sub>2</sub>O (Fig. 5, Fig. S5, Table S3).

Several polypeptides that almost do not exchange hydrogens for deuteriums, even within 120 min, were identified for all

three aSYN fibrillar polymorphs. The peptide 39 to 54, for example (Fig. S4A, dark gray box), exhibits an isotopic distribution close to that of the peptide incubated in H<sub>2</sub>O. We measured the incorporation of an average of 0.6 deuterium within this peptide after 30 min incubation of fibrils in deuterium. Considering the total number of exchangeable hydrogens (15) and the average back exchange (43%), the level of deuterium exchange is 7%. In contrast, peptide 95 to 113 appears labile and/or exposed to the solvent in monomeric and fibrillar aSYN polymorphs (Fig. S4B, light gray box).

Overall, the HDX measurements we performed demonstrate that aSYN amino acid stretch 95 to 140 is highly exposed to the solvent within all fibrillar polymorphs. This contrasts with aSYN N-terminal end that appears exposed till residues 38 or 17 in the polymorphs fibrils and fibrils 91, respectively, but not at all in the polymorph ribbons. (Fig. 5, Table S3). These findings are in full agreement with the differential antibodies accessibility and limited proteolysis data.

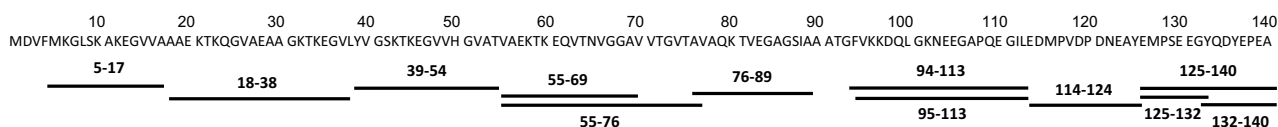
## Discussion

The structures, at an atomic resolution, of the core of several aSYN fibrillar polymorphs assembled *in vitro* or purified from the brain of patients and subjected to proteolytic treatments have been reported recently (25, 26, 33, 39–43). aSYN fibrillar polymorphs core density maps obtained by cryo-EM provide incomplete information on the amino acid stretches exposed to the solvent at the surface of the fibrillar polymorphs, in particular when those amino acid stretches are flexible. Identifying to the highest extent those surfaces is critical as it is through those surfaces that aSYN fibrillar polymorphs interact with their cellular partners (44) leading eventually to their pathogenic redistribution (15, 44). Using a combination of state-of-the-art methods that can yield information at an atomic resolution, namely differential accessibility of monoclonal antibodies, limited proteolysis and HDX measurements, we have mapped the surfaces of distinct aSYN fibrillar polymorphs.

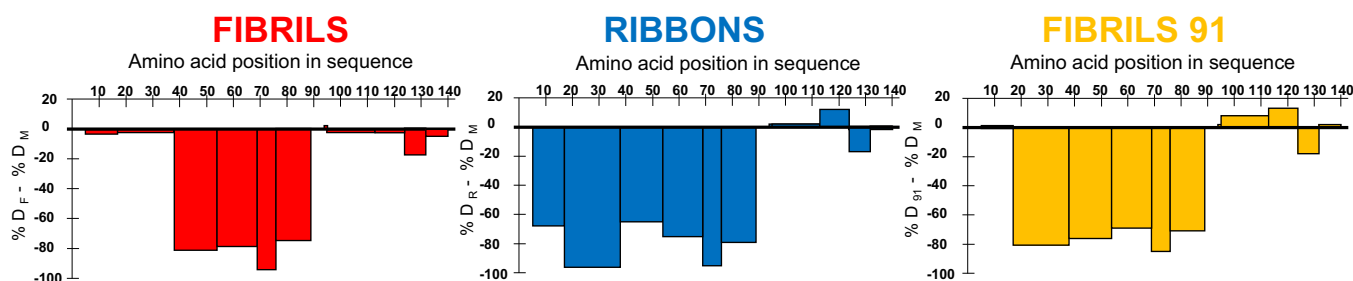
### aSYN fibrillar polymorphs surfaces

We show here that aSYN C-terminal amino acid stretch spanning 94 to 140 within all three aSYN polymorphs we

## A HDX sequence coverage of aSYN



## B HDX protection map upon assembly of the three aSYN strains



## C HDX protection map on aSYN sequence

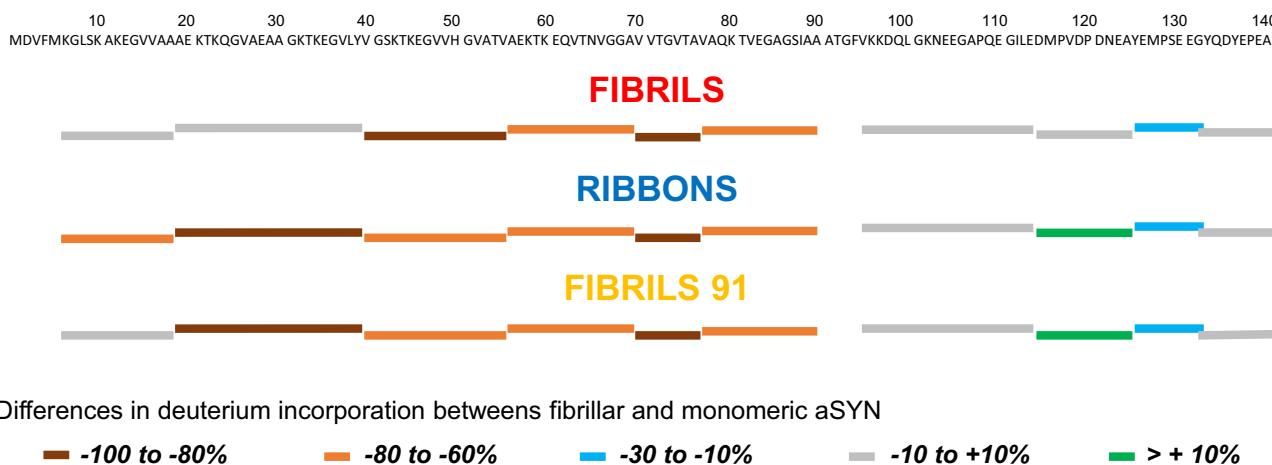


**Figure 5. Changes in the exposure of aSYN to the solvent upon assembly into distinct fibrillar polymorphs assessed by hydrogen-deuterium exchange.** A, sequence coverage of aSYN obtained by pepsin digestion and used for HDX experiments. B, HDX protection maps upon assembly of monomeric aSYN into the fibrillar polymorphs fibrils, ribbons, and fibrils 91 were obtained by measuring for each pepsin peptide the difference in deuterium incorporation in monomeric versus fibrillar aSYN polymorphs. C, HDX protection maps upon assembly of each aSYN into fibrils, ribbons, and fibrils 91 with color bars underlining aSYN primary structure showing the difference in deuterium incorporation upon assembly of monomeric aSYN into fibrillar polymorphs summarizes our findings. Regions in white are not covered. The data correspond to the average values of  $n = 3$  independent replicates, with a maximum standard deviation of 12% between replicates.

analyzed is highly exposed to the solvent. This is consistent with the solid-state NMR data we generated indicating that aSYN C-terminal end is flexible within those fibrillar polymorphs (27, 29, 30). Our results are also consistent with the two polymorph structures of aSYN fibrils solved by cryo-EM showing that the amino acid residues stretch 95 to 140 is dynamic and thus unresolved (33). The regions identified by HDX as exposed to the solvent within aSYN fibrils are larger than that delineated by limited proteolysis. This is due to the fact that proteases binding to protein substrates requires larger accessible polypeptide stretches.

Our limited proteolysis measurements show that PK and thermolysin cleave all fibrillar polymorphs at residues 113 or 125 and 111, respectively. Interestingly, the C-terminal complementary fragments (peptides 126-140 for proteinase K and 112-140 for thermolysin) were not progressively degraded into shorter polypeptides. This suggests that the proteases distinguish a subset of cleavage sites within aSYN C-terminal domain (residues 95-140) in the fibrils under our experimental conditions as a consequence cleavage at defined sites but not at others. This in turn suggests that aSYN amino acid stretch 112 to 140 exhibits a stable secondary structure incompatible with further degradation. aSYN C-terminal end

## Surface mapping of alpha-synuclein strains

may interact with the amino acid stretch centered on residue 36 from the partner protofilament within the two polymorph structures of aSYN fibrils we solved by cryo-EM (33) and has been proposed to play a role in protofilament–protofilament interaction within the fibrillar form of the protein (45, 46).

aSYN fibrillar polymorphs remained of fibrillar nature as assessed by TEM imaging after 15 min proteolysis. This suggests that the intra and intermolecular interactions within the fibrillar polymorphs hold the resulting proteolytic products together. Fibrillar aSYN polymorphs had a tendency to bundle after proteolysis, in a manner similar to fibrils assembled from C-terminally truncated aSYN (47–49). This is certainly due to the loss of the negatively charged C-terminal residues that repel the fibrils from one another.

We observed striking differences in aSYN N-terminal end exposure to the solvent in distinct fibrillar polymorphs. While aSYN N-terminal end was fully inaccessible to proteinase K and thermolysin, also highly protected in HDX measurements in ribbons it was found exposed to the solvent till amino acid residue 38 or 17 in the polymorphs fibrils and fibrils 91, respectively. These findings are consistent with those we reported previously using solid-state-NMR measurements (27, 29, 30) and illustrate the power of the approach we implemented to map structural polymorphism within amyloid fibrils. All the amino acid stretches we identify as accessible to proteases or undergoing rapid HDX are within regions we previously showed not to adopt a beta strand conformation except two, spanning residues 16 to 20 and 35 to 38 in aSYN polymorph fibrils. Albeit in beta strand conformations, these amino acid stretches appear at the surface of the fibrils based on the cryo-EM structures we solved (33) not in typical H-bonded structures constitutive of an amyloid core where slow HDX is observed.

### Impact of our findings on understanding distinct synucleinopathies and developing therapeutic and diagnostic tools

Mapping of the surfaces of pathologic aSYN fibrillar polymorphs to the highest possible resolution enables understanding how they interact with cellular components and through proteomic studies and *in silico* modeling the identification of their local interactomes. We report here structural differences and similarities between distinct fibrillar aSYN polymorphs. The finding that aSYN polypeptide stretch spanning residues 95 to 140 is accessible to antibodies, to proteases and exposed to the solvent in all fibrillar polymorphs suggests that this region does not allow distinguishing a fibrillar polymorph from another. It also suggests that the cellular interactome of this region is common in structurally distinct aSYN fibrillar polymorphs. This finding is in sharp contrast with what we report for aSYN N-terminal end. Indeed, the accessibility to antibodies, to proteases and exposure to the solvent of the polypeptide stretch spanning residues 1 to 38 allow discriminating distinct aSYN fibrillar polymorphs. The differential exposure of aSYN N-terminal polypeptide stretch to the solvent within fibrillar assemblies

suggests they have different interactomes and as a consequence distinct pathogenic functional properties and tropism for neuronal cells.

Altogether our results show that ligands of the C-terminal end of aSYN possess diagnostic potential for all synucleinopathies while ligands of aSYN N-terminal end allow distinguishing one synucleinopathy from another. In all cases, such ligands may hold therapeutic potential as they interfere with and may prevent the interaction between pathogenic assemblies and yet to be fully identified partners.

Further characterization of pathogenic aSYN assemblies derived from patients' brains using the strategy we implemented and identification of the generic and specific interactomes will lead to a better understanding of synucleinopathies and the design of ways to interfere with their prion-like propagation.

## Experimental procedures

### Production and assembly of recombinant aSYN

Recombinant aSYN production and assembly into the fibrillar polymorphs fibrils, ribbons, and fibrils 91 were performed as previously described (22, 28, 31, 50). Assembly was monitored using Thioflavin T as previously described (22). Monomeric alpha-synuclein concentration was determined spectrophotometrically using the extinction coefficients  $5960 \text{ M}^{-1} \cdot \text{cm}^{-1}$  at 280 nm. Samples used for limited proteolysis and antibodies accessibility were spun at 100,000g for 30 min after assembly. Fibrillar assemblies concentration was determined by subtracting the concentration of aSYN in the supernatant fraction from the initial protein concentration. The nature of aSYN fibrillar polymorphs was assessed using TEM as previously described (22).

### Limited proteolysis

Monomeric or fibrillar aSYN (1.4 mg/ml equivalent monomer concentration) was digested at 37 °C in PBS with Proteinase K (3.8 µg/ml) (Roche) or in 50 mM Tris pH8, 0.5 mM CaCl<sub>2</sub> with thermolysin (5 µg/ml) (Sigma). Aliquots were removed at different time intervals following addition of the protease (0, 1, 5, 15, 30, and 60 min) and transferred into Eppendorf tubes with proteinase K or thermolysin inhibitors (respectively PMSF: phenylmethylsulfonyl fluoride, or EDTA: ethylene diamine tetraacetic acid). Samples were dried using speed vacuum and further solubilized by addition of pure HFIP (Hexafluoroisopropanol). After evaporation of HFIP, the samples were resuspended in Laemmli buffer, heated 10 min at 70 °C, and processed for Tris-Glycine SDS-PAGE (12%) analysis.

### Western blot analysis

Samples subjected to Proteinase K or thermolysin treatment for 15 min and solubilized and subjected to SDS-PAGE analysis were transferred to nitrocellulose membranes. The membranes were blocked with 5% skimmed milk for 1 h, then incubated overnight with the antibodies ASyM (clone number 4.2, Agrisera, AS13 2719), 5G4, 10C3, or 10D2 (Analytic Jena,

ref 847-0102004001, 847-010200180 and 847-0102004701 respectively). The membranes were washed with Tris buffered saline with Tween 20 (20 mM Tris, 150 mM NaCl, 0.1% Tween 20) and incubated for 1 h with a goat anti-mouse IgG (GeneTex GTX 213111-01) coupled to HRP and imaged using a chemidoc imager (biorad). The membranes were stripped using 62.5 mM Tris/HCl pH 6.8, 2% SDS, 100 mM beta-ME (beta-mercaptoethanol) for 1 h at 50 °C prior to immunostaining a second time with the antibody Syn1 (Biosciences, Ref 610787).

#### Assessment of antibodies accessibility

Native monomeric fibrillar aSYN polymorphs (2.5 μM, 2 μl) were spotted in quadruplicate on a nitrocellulose membrane. The membrane was next blocked with 5% skimmed milk for 1 h and incubated with different antibodies as described above. For statistical analysis of the six replicates we performed, we assumed a Gaussian distribution and equal standard deviations for the intensities measured for each aSYN species and each antibody. We then performed one-way ANOVA followed by Dunnett's multiple comparisons test and compared the mean intensity obtained for each aSYN polymorph to the mean intensity obtained for monomeric aSYN, used as control, using GraphPad Prism (version 8.0.0 for Windows, GraphPad Software, [www.graphpad.com](http://www.graphpad.com)). Significant (\*\*\*\* corresponding to a *p*-value < 0.0001) and nonsignificant (ns corresponding to *p*-value > 0.05) differences are indicated.

#### Matrix-assisted laser desorption ionization mass spectrometry (MALDI-MS) measurements

The reaction products generated after 15 min treatment of aSYN monomers and fibrillar polymorphs were solubilized in HFIP as described above and 1:10 (for the analyses of long polypeptides, ranging from 4000 to 15,000 Da) or 1:20 (for the analyses of short polypeptides, ranging from 800 to 4000 Da) in trifluoroacetic acid (TFA 0.1%). Samples were subjected to MALDI-MS analysis, using Sinapinic acid (3,5-dimethoxy-4-hydroxycinnamic acid, Aldrich) or HCCA (α-cyano-4-hydroxycinnamic acid, Aldrich) as matrices for long and short peptides, respectively. Both matrices were prepared as saturated solutions in 50% acetonitrile (ACN) and 0.1% trifluoroacetic acid (TFA). The spectra were acquired on a MALDI-TOF/TOF 5800 (AB Sciex). Mass measurements were performed in linear or reflectron modes for long and short polypeptides, respectively. External mass calibration was achieved using full-length aSYN or Pepmix4, a mixture of bradykinin 1 to 5 (573.3149 Da), angiotensin II (1046.5423 Da), Neurotensin (1672.9175 Da), ACTH [18–39] (2465.1989 Da), and bovine insulin chain B (3494.6513 Da) from LaserBio Labs, in linear and reflectron mode, respectively. For long polypeptides, full-length aSYN present in the samples was further used for additional internal calibration. Identification of the peptides was performed using the GPMAW 8.2 software and a minimum mass difference between measured and theoretical masses set at 100 ppm in reflectron mode and 300 ppm in

linear mode. Three independent replicates were performed for each type of analysis.

#### Hydrogen/deuterium exchange experiments

The protocol we used was adapted from Redeker *et al.* (51). aSYN monomers and fibrillar polymorphs were treated in parallel. Hydrogen to deuterium exchange was initiated by diluting (1:20, *e.g.*, 2 μl of the protein sample (1.4 mg/ml) into 38 μl of 99.9% pure solution of D<sub>2</sub>O, (Aldrich)). To achieve an exchange kinetic in reproducible conditions, samples were then incubated at 20 °C for 2, 30, or 120 min. The exchange reaction was quenched by decreasing the temperature and the pH rapidly (0 °C, pH 2.5) by addition of 120 μl of an ice-cold solution of formic acid (3%) in water. The quenched samples (160 μl) were immediately further digested at 0 °C using molten ice by addition of 120 μl of immobilized pepsin (Thermo Scientific) at an enzyme to protein ratio 100:1 w/w. The digestion reactions were carried out for 2 min in the upper tail of an ultrafree-MC tube (Merck-Millipore, UFC30GV0S), and the reaction products were recovered in the tube by a short spin at 10,000g (30 s, 0 °C).

The pepsin-derived peptides (6 μl) were loaded onto a C18 Zip-Tip, desalted as previously described (51), spotted onto the MALDI plate under a nitrogen flow, and directly analyzed on a MALDI-TOF/TOF 5800 (AB Sciex). The spectra were acquired in the positive and reflectron ion mode in the *m/z* range 800 to 5000. An external mass calibration was applied using Pepmix4. Further internal calibration was performed using the sodium adduct of peptide 95 to 113 (*m/z* 2075.07), well characterized by MALDI MS/MS fragmentation (CID) as shown in Fig. S3. Mass difference between measured and theoretical masses was set at 50 ppm.

All spectra were analyzed using peak view software. As the peaks of peptides with sodium adduct have a better intensity, we first confirmed their identity by further desalting directly on the MALDI plate and by CID fragmentation using MALDI-TOF-TOF (Fig. S4). We completed this identification by nanoLC-MSMS with a TripleTOF 4600 (ABSciex) mass spectrometer as previously described (52). Peptides were identified using a database search with the Mascot search engine (Matrix Science, version 2.4.1) against the aSYN sequence and manual validation was performed.

We then analyzed HDX of those peptide peaks. The amount of hydrogen to deuterium exchange was calculated as previously described (51) except that the baseline correction was done directly on peak view software, using the height centroid spectrum option. The centroid mass value of the isotope distribution was calculated as:

$$\sum (\text{weighted areas} * \text{isotopic mass})$$

where the weighted area is the area of one isotope divided by the sum of the areas of all the isotopes composing the isotopic peak envelope, and the isotopic mass is the mass of the considered isotope.

## Surface mapping of alpha-synuclein strains

Back-exchange was measured using a 2 min pepsin digest of aSYN monomers obtained in the same conditions as those used for aSYN polymorphs (same protein concentration, same enzyme-to-protein ratio). The pepsin digest was vacuum dried. The dried pepsin-peptides sample was resuspended in a 99.9% pure solution of D2O and incubated during 24 h. The fully deuterated aSYN peptides were analyzed by MALDI-MS, under exactly the same dilutions and ice-cold incubations (2 min 30 s corresponding to quenching and ultra-free-MC tube spinning) and using exactly the same sample preparation as the one used for the HDX kinetics of aSYN monomers and polymorphs (2 min including desalting on a C18 Zip-Tip, spotting onto the MALDI plate, and complete drying under a nitrogen flow). Deuterium incorporation measured for the fully deuterated peptides was compared with the theoretical mass of the fully deuterated peptides. Using triplicate back-exchange experiments and six pepsin-derived aSYN peptides (5–17, 18–38, 39–54, 94–113, 114–124, and 125–140), we calculated an average back-exchange of 43% with a standard deviation of 3%.

All the experiments were done in triplicate. The data we present are those obtained after 30 min exchange in D2O when maximum deuterium incorporation is observed. The mean standard deviation is 4% and the maximum standard deviation measured is <12%.

### Data availability

All data are included in the article and supporting information.

**Supporting information**—This article contains [supporting information](#).

**Acknowledgments**—We thank Luc Bousset for assistance in TEM, and the Proteomic-Gif SICaPS platform (I2BC), supported by IBI SA, Ile de France Region, Plan Cancer, CNRS and Paris-Sud University, for allowing us to use their MS equipment and in particular Laïla Sago and David Cornu for their assistance. This work was supported by the Centre National de la Recherche Scientifique (CNRS), Institut National de la Santé et de la Recherche Médicale (Inserm), and a Convention Industrielle de Formation par la Recherche (CIFRE) from the Association Nationale de la recherche et de la technologie (ANRT). This work was supported by grants from the Fondation pour la Recherche Médicale (contract DEQ. 20160334896 and ALZ201912009776) and the EU Joint Programme on Neurodegenerative Disease Research and Agence National de la Recherche (contracts PROTEST-70, ANR-17-JPND-0005-01 and Trans-PathND, ANR-17-JPND-0002-02). This work has also received support from the European Union's Horizon 2020 research and innovation program and EFPIA Innovative Medicines Initiative 2 grant agreements No 116060 (IMPRiND) and No. 821522 (PD-MitoQUANT), the Swiss State Secretariat for Education, Research and Innovation (SERI) under contract number 17.00038, Parkinson UK and SANOFI.

**Author contributions**—M. L. performed experiment (Syn purification, assembly, limited proteolysis, HDX, MS), analyzed the data, and wrote the article. V. R. designed the work, performed the

experiments (MS), analyzed the data, wrote article. T. B. performed the experiments (biochemistry and gel electrophoresis). S. E. designed the work. R. M. designed and directed the work, wrote the article.

**Conflict of interest**—S. E. is full-time employee of SANOFI R&D.

**Abbreviations**—The abbreviations used are: CID, Collision-induced dissociation; cryo-EM, cryo-electron microscopy; D2O, deuterium; DLB, dementia with Lewy bodies; EDTA, ethylene diamine tetraacetic acid; HCCA,  $\alpha$ -cyano-4-hydroxycinnamic acid; HDX-MS, hydrogen-deuterium exchange mass spectrometry; HFIP, hexafluoroisopropanol; MALDI-TOF, matrix-assisted laser desorption/ionization time-of-flight; MSA, multiple system atrophy; NAC, nonamyloid- $\beta$  component; nanoLC-MS/MS, nanoflow liquid chromatography combined to tandem mass spectrometry; NMR, nuclear magnetic resonance; PD, Parkinson's disease; PMSF, phenyl methyl sulfonyl fluoride; SDS-PAGE, sodium dodecyl sulfate-polyacrylamide gel electrophoresis; TEM, transmission electron microscopy; TFA, trifluoroacetic acid.

### References

1. Spillantini, M. G., Crowther, R. A., Jakes, R., Hasegawa, M., and Goedert, M. (1998) Alpha-synuclein in filamentous inclusions of Lewy bodies from Parkinson's disease and dementia with Lewy bodies. *Proc. Natl. Acad. Sci. U. S. A.* **95**, 6469–6473
2. Goedert, M. (2001) Alpha-synuclein and neurodegenerative diseases. *Nat. Rev. Neurosci.* **2**, 492–501
3. Jakes, R., Spillantini, M. G., and Goedert, M. (1994) Identification of two synucleins from human brain. *FEBS Lett.* **345**, 27–32
4. Burré, J., Sharma, M., Tsetsenis, T., Buchman, V., Etherton, M. R., and Südhof, T. C. (2010)  $\alpha$ -synuclein promotes SNARE-complex assembly *in vivo* and *in vitro*. *Science* **329**, 1663–1667
5. Burré, J. (2015) The synaptic function of  $\alpha$ -synuclein. *J. Parkinsons Dis.* **5**, 699–713
6. Davidson, W. S., Jonas, A., Clayton, D. F., and George, J. M. (1998) Stabilization of alpha-synuclein secondary structure upon binding to synthetic membranes. *J. Biol. Chem.* **273**, 9443–9449
7. Eliezer, D., Kutluay, E., Bussell, R., Jr., and Browne, G. (2001) Conformational properties of alpha-synuclein in its free and lipid-associated states. *J. Mol. Biol.* **307**, 1061–1073
8. Rodriguez, J. A., Ivanova, M. I., Sawaya, M. R., Cascio, D., Reyes, F., Shi, D., Sangwan, S., Guenther, E. L., Johnson, L. M., Zhang, M., Jiang, L., Arbing, M. A., Nannega, B., Hattne, J., Whitelegge, J., *et al.* (2015) Structure of the toxic core of  $\alpha$ -synuclein from invisible crystals. *Nature* **525**, 486–490
9. Binolfi, A., Rasia, R. M., Bertoncini, C. W., Ceolin, M., Zweckstetter, M., Griesinger, C., Jovin, T. M., and Fernandez, C. O. (2006) Interaction of  $\alpha$ -synuclein with divalent metal ions reveals key differences: A link between structure, binding specificity and fibrillation enhancement. *J. Am. Chem. Soc.* **128**, 9893–9901
10. Alam, P., Bousset, L., Melki, R., and Otzen, D. E. (2019)  $\alpha$ -Synuclein and fibrils: A spectrum of species, a spectrum of toxicities. *J. Neurochem.* **150**, 522–534
11. Jucker, M., and Walker, L. C. (2013) Self-propagation of pathogenic protein aggregates in neurodegenerative diseases. *Nature* **501**, 45–51
12. Brundin, P., Melki, R., and Kopito, R. (2010) Prion-like transmission of protein aggregates in neurodegenerative diseases. *Nat. Rev. Mol. Cell Biol.* **11**, 301–307
13. Melki, R. (2018) How the shapes of seeds can influence pathology. *Neurobiol. Dis.* **109**, 201–208
14. Oosawa, F., and Asakura, S. (1975) *Thermodynamics of the Polymerization of Protein*, Academic Press, London, UK
15. Shrivastava, A. N., Aperia, A., Melki, R., and Triller, A. (2017) Physico-pathologic mechanisms involved in neurodegeneration: Misfolded protein-plasma membrane interactions. *Neuron* **95**, 33–50

16. De Mattos, E. P., Wentink, A., Nussbaum-Krammer, C., Hansen, C., Bergink, S., Melki, R., and Kampinga, H. H. (2020) Protein quality control pathways at the crossroad of synucleinopathies. *J. Parkinsons Dis.* **10**, 369–382
17. Flavin, W. P., Bousset, L., Green, Z. C., Chu, Y., Skarpathiotis, S., Chaney, M. J., Kordower, J. H., Melki, R., and Campbell, E. M. (2017) Endocytic vesicle rupture is a conserved mechanism of cellular invasion by amyloid proteins. *Acta Neuropathol.* **134**, 629–653
18. Gustot, A., Gallea, J. I., Sarroukh, R., Celej, M. S., Ruyschaert, J. M., and Raussens, V. (2015) Amyloid fibrils are the molecular trigger of inflammation in Parkinson's disease. *Biochem. J.* **471**, 323–333
19. Yamasaki, T. R., Holmes, B. B., Furman, J. L., Dhavale, D. D., Su, B. W., Song, E. S., Cairns, N. J., Kotzbauer, P. T., and Diamond, M. I. (2019) Parkinson's disease and multiple system atrophy have distinct  $\alpha$ -synuclein seed characteristics. *J. Biol. Chem.* **294**, 1045–1058
20. McCann, H., Stevens, C. H., Cartwright, H., and Halliday, G. M. (2014)  $\alpha$ -Synucleinopathy phenotypes. *Parkinsonism Relat. Disord.* **20S1**, S62–S67
21. Chien, P., Weissman, J. S., and DePace, A. H. (2004) Emerging principles of conformation-based prion inheritance. *Annu. Rev. Biochem.* **73**, 617–656
22. Bousset, L., Pieri, L., Ruiz-Arlandis, G., Gath, J., Henning Jensen, P., Habenstein, B., Madiona, K., Olieric, V., Böckmann, A., Meier, B. H., and Melki, R. (2013) Structural and functional characterization of two alpha-synuclein strains. *Nat. Commun.* **4**, 2575
23. Peelaerts, W., Bousset, L., Van der Perren, A., Moskalyuk, A., Pulizzi, M., Van den Haute, C., Melki, R., and Baekelandt, V. (2015)  $\alpha$ -Synuclein strains cause distinct synucleinopathies after local and systemic administration. *Nature* **522**, 340–344
24. Shahnawaz, M., Mukherjee, A., Pritzkow, S., Mendez, N., Rabadia, P., Liu, X., Smeichel, A., Singer, W., Wu, G., Tsai, A. L., Shirani, H., Nilsson, P. R., Low, P. A., and Soto, C. (2020) Discriminating  $\alpha$ -synuclein strains in Parkinson's disease and multiple system atrophy. *Nature* **578**, 273–277
25. Strohäker, T., Jung, B. C., Liou, S. H., Fernandez, C. O., Riedel, D., Becker, S., Halliday, G. M., Bennati, M., Kim, W. S., Lee, S. J., and Zwecksteter, M. (2019) Structural heterogeneity of  $\alpha$ -synuclein fibrils amplified from patient brain extracts. *Nat. Commun.* **10**, 535
26. Van der Perren, A., Gelders, G., Fenyi, A., Bousset, L., Brito, F., Peelaerts, W., Van den Haute, C., Gentleman, S., Melki, R., and Baekelandt, V. (2020) The structural differences between patient-derived  $\alpha$ -synuclein strains dictate characteristics of Parkinson's disease, multiple system atrophy and dementia with Lewy bodies. *Acta Neuropathol.* **139**, 977–1000
27. Verasdonck, J., Bousset, L., Gath, L., Melki, R., Böckmann, A., and Meier, B. H. (2016) Further exploration of the conformational space of  $\alpha$ -synuclein fibrils: Solid-state NMR assignment of a high-pH polymorph. *Biomol. NMR Assign.* **10**, 5–12
28. Makky, A., Bousset, L., Polesel-Mariss, J., and Melki, R. (2016) Nano-mechanical properties of distinct fibrillar polymorphs of the protein  $\alpha$ -synuclein. *Sci. Rep.* **6**, 37970
29. Gath, J., Habenstein, B., Bousset, L., Melki, R., Meier, B. H., and Böckmann, A. (2012) Solid-state NMR sequential assignments of  $\alpha$ -synuclein. *Biomol. NMR Assign.* **6**, 51–55
30. Gath, J., Bousset, L., Habenstein, B., Melki, R., Böckmann, A., and Meier, B. H. (2014) Unlike twins: An NMR comparison of two  $\alpha$ -synuclein polymorphs featuring different toxicity. *PLoS One* **9**, e90659
31. Shrivastava, A. N., Bousset, L., Renner, M., Redeker, V., Savistchenko, J., Triller, A., and Melki, R. (2020) Differential membrane binding and seeding of distinct  $\alpha$ -synuclein fibrillar polymorphs. *Biophys. J.* **118**, 1–20
32. Rey, N. L., Bousset, L., George, S., Madan, Z., Meyerdirk, L., Schulz, E., Steiner, J. A., Melki, R., and Brundin, P. (2019)  $\alpha$ -Synuclein conformational strains spread, seed and target neuronal cells differentially after injection into the olfactory bulb. *Acta Neuropathol. Commun.* **7**, 221–238
33. Guerrero-Ferreira, R., Taylor, N. M., Arteni, A. A., Kumari, P., Mona, D., Ringler, P., Britschgi, M., Lauer, M. E., Makky, A., Verasdonck, J., Riek, R., Melki, R., Meier, B. H., Böckmann, A., Bousset, L., et al. (2019) Two new polymorphic structures of human full-length alpha-synuclein fibrils solved by cryo-electron microscopy. *Elife* **8**, e48907
34. Fontana, A., Polverino de Laureto, P., Spolaore, B., Frare, E., Picotti, P., and Zamboni, M. (2004) Probing protein structure by limited proteolysis. *Acta Biochim. Pol.* **51**, 299–321
35. de Laureto, P. P., Tosatto, L., Frare, E., Marin, O., Uversky, V. N., and Fontana, A. (2006) Conformational properties of the SDS-bound state of alpha-synuclein probed by limited proteolysis: Unexpected rigidity of the acidic C-terminal tail. *Biochemistry* **45**, 11523–11531
36. Zhang, Z., and Smith, D. L. (1993) Determination of amide hydrogen exchange by mass spectrometry: A new tool for protein structure elucidation. *Protein Sci.* **2**, 522–531
37. Illes-Toth, E., Rempel, D. L., and Gross, M. L. (2018) Pulsed hydrogen-deuterium exchange illuminates the aggregation kinetics of  $\alpha$ -synuclein, the causative agent for Parkinson's disease. *ACS Chem. Neurosci.* **9**, 1469–1476
38. Perrin, R. J., Payton, J. E., Barnett, D. H., Wraight, C. L., Woods, W. S., Ye, L., and George, J. M. (2003) Epitope mapping and specificity of the anti-alpha-synuclein monoclonal antibody Syn-1 in mouse brain and cultured cell lines. *Neurosci. Lett.* **349**, 133–135
39. Li, Y., Zhao, C., Luo, F., Liu, Z., Gui, X., Luo, Z., Zhang, X., Li, D., Liu, C., and Li, X. (2018) Amyloid fibril structure of  $\alpha$ -synuclein determined by cryo-electron microscopy. *Cell Res.* **28**, 897–903
40. Li, B., Ge, P., Murray, K. A., Sheth, P., Zhang, M., Nair, G., Sawaya, M. R., Shin, W. S., Broyer, D. R., Ye, S., Eisenberg, D. S., Zhou, Z. H., and Jiang, L. (2018) Cryo-EM full-length  $\alpha$ -synuclein reveals fibril polymorphs with a common structural kernel. *Nat. Commun.* **9**, 3609
41. Sun, Y., Hou, S., Zhao, K., Long, H., Liu, Z., Gao, J., Zhang, Y., Su, X. D., Li, D., and Liu, C. (2020) Cryo-EM structure of full-length alpha-synuclein amyloid fibril with Parkinson's disease familial A53T mutation. *Cell Res.* **30**, 360–362
42. Zhao, K., Li, Y., Liu, Z., Long, H., Zhao, C., Luo, F., Sun, Y., Tao, Y., Su, X. D., Li, D., Li, X., and Liu, C. (2020) Parkinson's disease associated mutation E46K of alpha-synuclein triggers the formation of a distinct fibril structure. *Nat. Commun.* **11**, 2643
43. Zhao, K., Lim, Y. J., Liu, Z., Long, H., Sun, Y., Hu, J. J., Zhao, C., Tao, Y., Zhang, X., Li, D., Li, Y. M., and Liu, C. (2020) Parkinson's disease-related phosphorylation at Tyr39 rearranges alpha-synuclein amyloid fibril structure revealed by cryo-EM. *Proc. Natl. Acad. Sci. U. S. A.* **117**, 20305–20315
44. Shrivastava, A. N., Redeker, V., Fritz, N., Pieri, L., Almeida, L. G., Spolidoro, M., Liebmann, T., Bousset, L., Renner, M., Léna, C., Aperia, A., Melki, R., and Triller, A. (2015)  $\alpha$ -Synuclein assemblies sequester neuronal  $\alpha$ 3-Na<sup>+</sup>/K<sup>+</sup>-ATPase and impair Na<sup>+</sup> gradient. *EMBO J.* **34**, 2408–2423
45. Qin, Z., Hu, D., Han, S., Hong, D. P., and Fink, A. L. (2007) Role of different regions of  $\alpha$ -synuclein in the assembly of fibrils. *Biochemistry* **46**, 13322–13330
46. Hong, D. P., Xiong, W., Chang, J. Y., and Jiang, C. (2011) The role of the C-terminus of human  $\alpha$ -synuclein: Intra disulfide bonds between the C-terminus and other regions stabilize non-fibrillar monomeric isomers. *FEBS Lett.* **585**, 561–566
47. Ma, L., Yang, C., Zhang, X., Li, Y., Wang, S., Zheng, L., and Huang, K. (2018) C-terminal truncation exacerbates the aggregation and cytotoxicity of  $\alpha$ -synuclein: A vicious cycle in Parkinson's disease. *Biochim. Biophys. Acta Mol. Basis Dis.* **1864**, 3714–3725
48. Van der Wateren, I. M., Knowles, T. P. J., Buell, A. K., Dobson, C. M., and Galvagnion, C. (2018) C-terminal truncation of  $\alpha$ -synuclein promotes amyloid fibril amplification at physiological pH. *Chem. Sci.* **9**, 5506–5516
49. Gallardo, J., Escalona-Noguero, C., and Sot, B. (2020) Role of  $\alpha$ -synuclein regions in nucleation and elongation of amyloid fibre assembly. *ACS Chem. Neurosci.* **11**, 872–879
50. Ghee, M., Melki, R., Michot, N., and Mallet, J. (2005) PA700, the regulatory complex of the 26S proteasome, interferes with alpha-synuclein assembly. *FEBS J.* **272**, 4023–4033
51. Redeker, V., Halgand, F., Le Caer, J. P., Bousset, L., Laprèvote, O., and Melki, R. (2007) Hydrogen/Deuterium exchange mass spectrometric analysis of conformational changes accompanying the assembly of the yeast prion Ure2p into protein fibrils. *J. Mol. Biol.* **369**, 1113–1125
52. Bendifallah, M., Redeker, V., Monsellier, E., Bousset, L., Bellande, T., and Melki, R. (2020) Interaction of the chaperones alpha B-crystallin and CHIP with fibrillar alpha-synuclein: Effects on internalization by cells and identification of interacting interfaces. *Biochem. Biophys. Res. Commun.* **527**, 760–769